Determination of the local conformation of PMMA from wide-angle X-ray scattering

Richard Lovell and Alan H. Windle
Department of Metallurgy and Materials Science, University of Cambridge, Pembroke Street, Cambridge CB2 3QZ, UK
(*Received* 29 *October* 1979)

Detailed conclusions about the local conformational structure of atactic PMMA have been derived from WAXS. The underlying conformation is near to the all-*trans* energy minimum proposed by Sundararajan and Flory. Precise values of backbone rotation angles (10°, 10°, −10°, −10°) and bond angles (110° and 128°) confirm the prediction that the chain consists of curved segments. The regular conformation persists over 16–20 backbone bonds for syndiotactic PMMA, and its curvature may explain why s-PMMA cannot be thermally crystallized.

INTRODUCTION

The conformational structure of solid non-crystalline polymers is usually derived from measurements of infrared (i.r.) spectra or of nuclear magnetic resonance (n.m.r.). The details are rather imprecise, usually being expressed as a preference for one of the staggered-bond conformations. Here, we report a wide-angle X-ray scattering (WAXS) study on atactic poly(methyl methacrylate) (a-PMMA) which leads to detailed conclusions about the conformation.

For crystalline polymers, WAXS is the preferred technique for determining structure, whereas its application to non-crystalline polymers has been much less successful. The usual approach has been to transform the X-ray scattering into the radial distribution function (*RDF*)[1,2]. However, the interpretation of *RDFs* in terms of the underlying conformation present (if any) is far from straightforward since the region of interest (3–5 Å) usually contains both inter- and intra-molecular distances[3]. A more sensitive method is to compare the experimental scattering with that calculated for models, that is to work in reciprocal space rather than in real space[4,5]. Such a technique depends on the ability to separate the experimental scattering into inter- and intramolecular contributions. For glassy polymers, this can be achieved by orienting specimens at temperatures just below the glass transition.

If such separation is made then the data can be compared with the scattering calculated for sterically reasonable models of single chains. For polymers such as PMMA with fairly rigid chains, we can use short regular conformations as suitable models. The number of different conformations that need be considered can be limited by using published conformational energy calculations to exclude unrealistic ones. Thus the technique combines qualitative steric information with WAXS data.

Previous evidence on the conformation of a-PMMA is rather inconclusive. The *RDF* derived from WAXS has been interpreted[1] in terms of a 'non-planar zig-zag' with an axial repeat of 4.7 Å. However, small-angle neutron scattering from deuterated specimens[6] has been explained on the basis that the molecule has a predominantly *trans* conformation but with curved segments due to unequal backbone bond angles[7]. I.r. measurements on s-PMMA[8] and on model compounds[9] are in agreement with a planar zig-zag. Evidence on the conformation of s-PMMA in solution has been reviewed by Inoue and Konno[10]. From their own n.m.r. measurements they conclude that the conformation depends on the nature of the solvent.

Establishment of an agreed conformational structure for a-PMMA is an important step in understanding the amorphous state and forms a base for subsequent consideration of molecular packing. It also provides a foundation for methods of orientation measurement such as birefringence, i.r. dichroism and n.m.r. which need to assume an underlying conformation.

EXPERIMENTAL

The materials used in this investigation were commercial atactic PMMA (ICI Perspex) and highly syndiotactic PMMA (96% racemic dyads).

The diffracted intensity for unoriented specimens is shown in *Figure 1*. This was collected using a symmetrical reflection diffractometer with MoKα radiation. The patterns for the two materials are very similar. Although the first two peaks are clearly shown in the raw data, the features at higher values of s are more easily seen in the reduced intensity function, $si(s)$, where

$$i(s) = kI(s) - \Sigma f^2(s) \qquad (1)$$

k is a scaling factor (to electron units), $I(s)$ is the fully corrected coherent intensity and $\Sigma f^2(s)$ is the independent scattering from one unit of composition. The correction and scaling of raw intensity data have been discussed elsewhere[11]. *Figure 2* shows the reduced intensity for atactic PMMA.

The structure of crystalline polymers is usually determined from the diffraction patterns of oriented fibres. Similarly, for glassy polymers, more information about the structure can be derived from the scattering from oriented samples. Specimens of a-PMMA were

0032 3861/81/020175 10$02.00

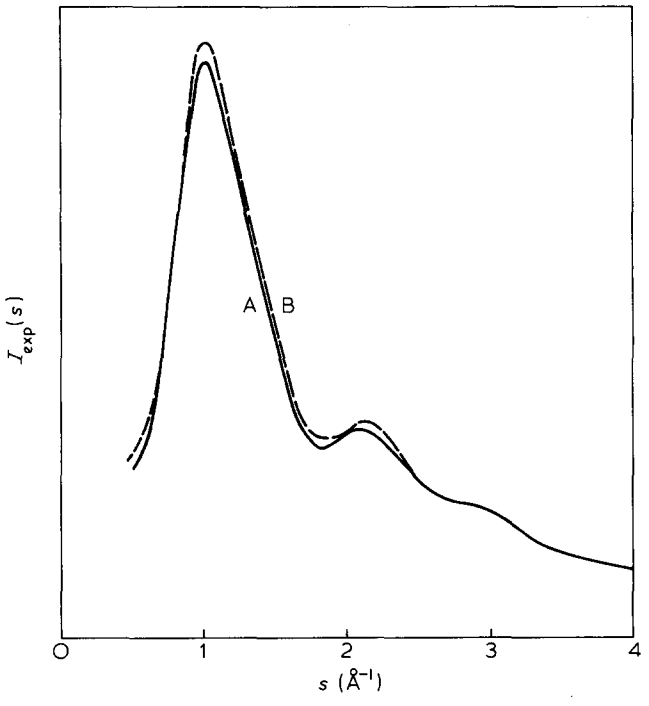

Figure 1 Uncorrected WAXS from (A) a-PMMA and (B) quenched s-PMMA. $s = (4\pi \sin\theta)/\lambda$

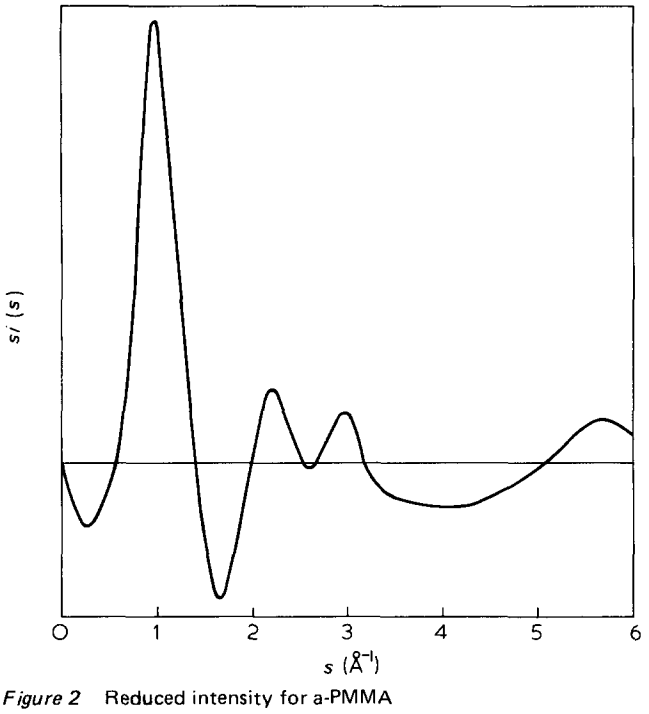

Figure 2 Reduced intensity for a-PMMA

oriented by extrusion in a channel die at 100°C. The deformation introduced corresponds to a draw ratio of about 3:1. *Figure 3* shows the scattering from such a specimen presented in the form $si(s, \psi)$ where

$$i(s, \psi) = kI(s, \psi) - \Sigma f^2(s)$$

and ψ is the azimuthal angle measured from the equator. The data were collected using a symmetrical transmission diffractometer fitted with an Eulerian cradle to rotate the specimen in its own plane[12]. CuKα-radiation was used and the incident intensity enhanced by a doubly-focussing LiF monochromator in the direct beam. The scaling factor, k, was obtained by normalizing an azimuthally averaged version of the data.

Meridional and equatorial sections of the oriented pattern, are shown in *Figure 4*. These indicate that the first halo is predominantly equatorial (i.e. due to intermolecular scattering), though there is a small meridional component at slightly higher s. The second and third peaks are purely meridional corresponding to periodicities along the polymer chains.

To find more accurately the positions of intramolecular peaks, we have previously applied an azimuthal sharpening technique to atactic and isotactic polystyrene[12]. Oriented specimens of these polymers give a purely equatorial halo with a sharp azimuthal profile and this

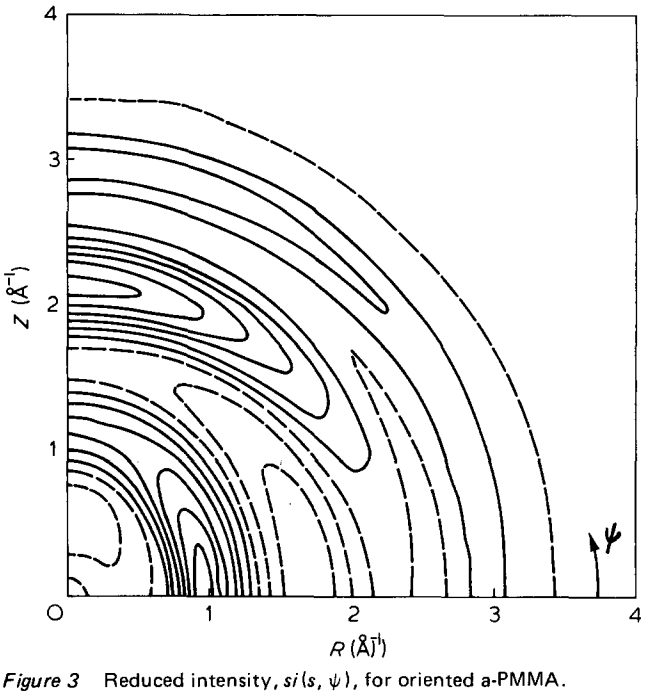

Figure 3 Reduced intensity, $si(s, \psi)$, for oriented a-PMMA. $R = s\cos\psi$, $Z = s\sin\psi$. Broken contours are negative

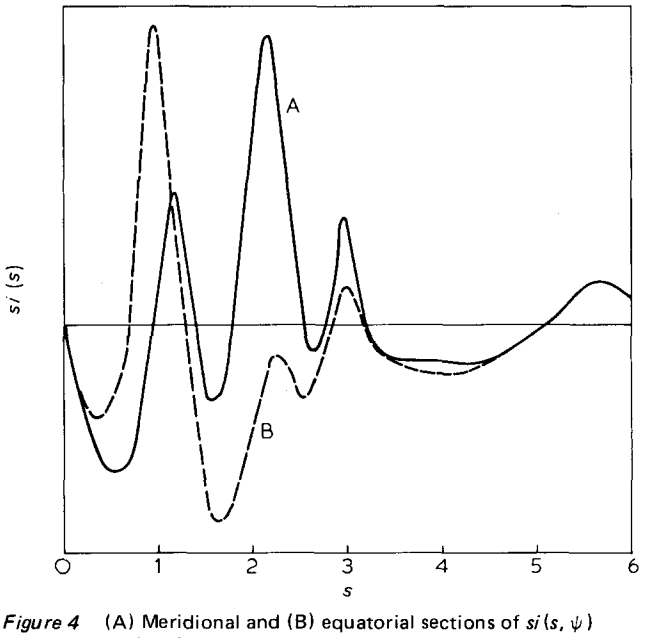

Figure 4 (A) Meridional and (B) equatorial sections of $si(s, \psi)$ for oriented a-PMMA

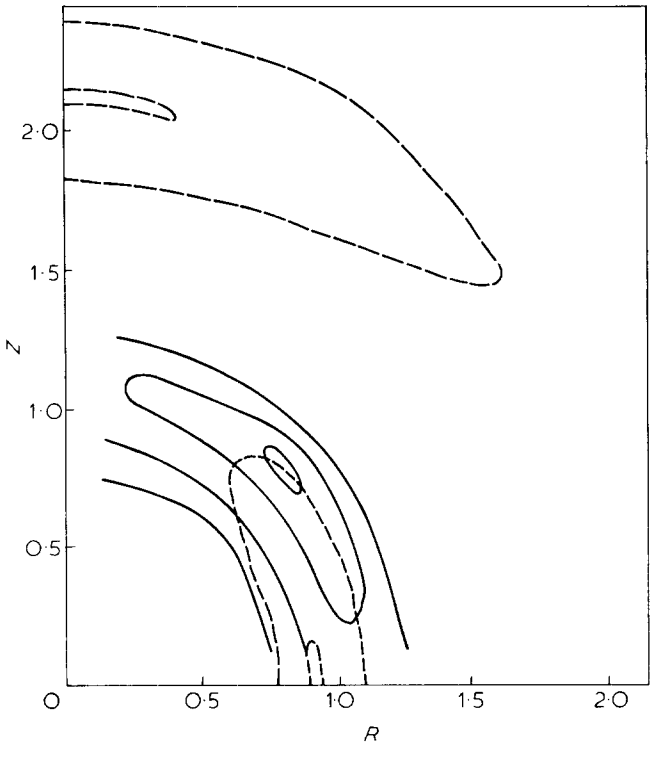

Figure 5 Azimuthally sharpened scattering data for oriented a-PMMA. The broken contours represent the position of the first and second maxima in the scattering pattern prior to sharpening

was used as the sharpening function. However, a-PMMA does not give such a well-defined feature and so it was necessary to use the azimuthal profile at $s = 0.7$ Å^{-1}, that is on the low s side of the first halo, thus avoiding the meridional component. Since most of the azimuthal profiles are similar in shape to the sharpening one, the deconvolution process is unstable and does not produce good results. However, in *Figure 5*, we show a somewhat schematic diagram of the sharpened data. This suggests that the higher s component of the first halo is in fact off-meridional[13].

Before comparing these experimental findings with the results of calculations for models, we first consider the steric information which restricts the number of conformations that need be considered.

AVAILABLE STERIC INFORMATION

The chemical structure of PMMA is shown in *Figure 6*. Nuclear magnetic resonance measurements have established that all but a small fraction of the monomer units are added in a head-to-tail fashion[14]. However, as with all vinyl polymers, this addition can occur in two ways, forming either a meso (m) dyad or a racemic (r) dyad. In atactic PMMA both types of dyad occur. N.m.r. can be used to determine the relative proportions of the three possible triads (isotactic: mm, heterotactic: rm, syndiotactic: rr) and hence the proportion of dyads[14]. For free-radical PMMA it has been found[15,16] that the triad ratios are compatible with addition obeying Bernoulli statistics (each monomer adds independently of the preceding one) with a probability of a racemic dyad, $P_r = 0.75$–0.80.

Taking $P_r = 0.75$, we can calculate that about 30% of the material is in runs of racemic dyads at least 8 units long. This predominance of syndiotactic sequences is confirmed by the marked similarity we have found between the WAXS patterns from a-PMMA and from quenched s-PMMA (*Figure 1*).

In the remainder of this paper, the structure of a-PMMA is analysed in terms of syndiotactic chain conformations.

In common with any structural analysis, whether dealing with crystalline or amorphous substances, it is necessary to incorporate steric information, such as atom sizes, bond angles and bond lengths, before the X-ray scattering data is able to indicate a definite structure.

Such steric information is available as space-filling models, the manipulation of which can show conformations that are totally impossible due to atomic overlap. Models however, can only be used as a general guide and more exact steric information must be obtained from calculations based on interatomic potentials. Calculated conformational energy maps for short lengths of syndiotactic chains have been published by Grigoreva, Birshtein and Gotlib[17], by Tanaka and Ishida[18] and by Sundararajan and Flory[19]. In each case the energies are plotted as contours on a map with rotation angles of two backbone bonds (φ_1 and φ_2) as coordinates. In Sundararajan and Flory's work φ_1 and φ_2 are the angles shown in *Figure 6*, whereas the other groups examine conformations of the form $(0°, \varphi_1, 0°, -\varphi_1)$ and $(\varphi_1, \varphi_1, \varphi_2, \varphi_2)$.

Each group of authors predicts a different lowest-energy conformation: $(0°, 150°, 0°, -150°)$[17], $(0°, 0°, 140°, 140°)$[18] and $(10°, 10°, -10°, -10°)$[19]. It is apparent that opening out of alternate backbone bond angles (θ_2 in *Figure 6*), so as to bend the molecule and provide more room for the ester and α-methyl groups, tends to favour the conformations near all-*trans*. Sundararajan and Flory's bond angles were $\theta_1 = 110°$ and $\theta_2 = 122°$, although Grigoreva *et al.* find $(10°, 10°, -10°, -10°)$ to be the next most stable minimum on the basis of equal bond angles of 114°.

As the first step in the WAXS analysis of PMMA, we have not confined ourselves to the lowest minimum suggested by conformational energy calculations, but have explored all reasonable conformational sequences of the general form $(\varphi_1, \varphi_2, \varphi_3, \varphi_4)$ where $\varphi = 0°$ or $\pm 120°$. These conformations, based on the five staggered-bond dyads (excluding $g\bar{g}$), are listed in *Table 1*. The underlying conformation will almost certainly approximate to one of these.

DETERMINATION OF STRUCTURE

Calculation of scattering

Atomic coordinates for the various models are calculated from backbone bond angles and rotation angles

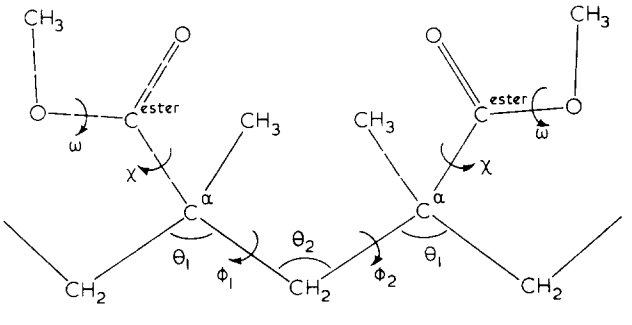

Figure 6 Chemical structure of a racemic dyad of PMMA. All rotation angles are shown as zero

Table 1 Staggered-bond conformations. Energy increasing from left to right and from top to bottom

1 \ 2	*tt*	$t\bar{g}$	$\bar{g}\bar{g}$	*tg*	*gg*
tt	*tttt*	$ttt\bar{g}$	$tt\bar{g}\bar{g}$	*tttg*	*ttgg*
tg		$tgt\bar{g}$	$tg\bar{g}\bar{g}$	*tgtg*	*tggg*
gg			$\frac{gggg}{\text{Ring}}$	*ggtg*	*gggg*
$t\bar{g}$				$t\bar{g}tg$	$t\bar{g}gg$
$\bar{g}\bar{g}$					$\frac{\bar{g}\bar{g}gg}{\text{Ring}}$

using a computer routine. Other bond angles and lengths have been fixed at the values used by Sundararajan and Flory[19] (except that all C–C = 1.54 Å and C$\hat{O}$C = 114°).

The spherically averaged scattering, $si(s)$, is then calculated using the Debye equation[20]:

$$i(s) = \sum_{j \neq k} \sum_{k} f_j(s) f_k(s) \frac{\sin r_{jk}s}{r_{jk}s}$$

where r_{jk} is the separation of the jth and kth atoms. Omission of the $j=k$ terms removes the independent scattering (Σf^2) as in equation (1). The methyl groups have been treated as single scattering units using the analytic fit to $f_{Me}(s)$ due to Narten[21]. The scattering factor for neutral hydrogen atoms was used for the non-methyl hydrogens. However, omitting all the hydrogen atoms has very little effect on the scattering beyond $s = 1.5$ Å^{-1}.

Owing to the small size of the models, there is a large peak in $i(s)$ centred at the origin and extending out to $s = 1.0$ Å^{-1}. This is effectively the scattering from a region the same size and shape as the model but containing randomly distributed atoms. Here, we are mainly concerned with the scattering beyond $s = 1.5$ Å^{-1}, and hence we have not taken steps to compensate for the small angle scattering.

Broad conformational type

Figure 7 shows the experimental $si(s)$ curves for unoriented PMMA and for the meridional scan of oriented PMMA. The intramolecular peaks are marked at $s \approx 1.15$ 2.15, 2.95, (3.9) and 5.7 Å^{-1}.These peaks can be compared with those in the scattering calculated for various conformations in *Figure 8*. These conformations are from *Table 1* and are based on perfectly staggered bonds. Those containing more than two *gauche* bonds have been omitted since even the ones that do not form rings will have very high steric hindrance.

The effect of increasing length of regular conformation is seen by comparing *Figures 8a* and *8b*. As would be expected, longer regular sequences give sharper peaks in $si(s)$. A more precise estimate of the run length will be discussed later; for the moment we adopt a length of 20 backbone bonds since this gives features about as sharp as in the data.

Figure 8b shows that all-*trans* (*tttt*) is the only conformation giving anything like reasonable agreement with experiment. We therefore examine the region near all-*trans* in greater detail.

Backbone bond angles

The scattering is particularly sensitive to changes in backbone bond angles (*Figure 9*) for conformations near all-*trans*, since unequal angles cause the chain to bend.

An all-*trans* chain with $\theta_1 = \theta_2$ is a planar zig-zag and the marked linear periodicity of a 25 Å length of such a chain shows up as sharp, triangular peaks corresponding to the layer lines of the infinite chain.

An all-*trans* chain with $\theta_1 < \theta_2$ forms an arc with the substituents pointing outwards, thus relieving the steric hindrance of adjacent sidegroups. Such chains give scattering with the peak near 2.5 Å^{-1} split into two components near 2.2 and 3.0 Å^{-1} as found experimentally for a-PMMA. The positions of the two peaks are in best agreement with experiment when θ_1 is 110° and θ_2 is 128°, and so we adopt these values for the backbone bond angles.

Refinement of rotation angles

The likely departures from all-*trans* give conformations which we have called types I and II[22]. In a type I conformation, all dyads are equivalent, i.e. (φ_1, φ_2, $-\varphi_1$, $-\varphi_2$), and in general the chain will form an arc. However, in a type II conformation, i.e. (φ_1, φ_1, φ_2, φ_2), the dyads are of two sorts but the C$^\alpha$ atoms are equivalent and in general the chain forms a helix. Conformations of the form (φ, φ, $-\varphi$, $-\varphi$) belong to both types. These type I/II chains generally form arcs.

In *Figure 10* we show scattering for four conformations near all-*trans*, one is of type I, two are of type I/II (all three form arcs), whereas the fourth is of type II and forms approximately a 5/1 helix (10 monomers in 1 turn). Both (0°, 20°, 0°, −20°) and (20°, 20°, −20°, −20°) give peaks near 1.2, 2.2 and 2.95 Å^{-1}. *Figure 11* shows other type I/II conformations with φ ranging from 0° to 25°. It can be seen that the best agreement is for $\varphi = 5$–10°.

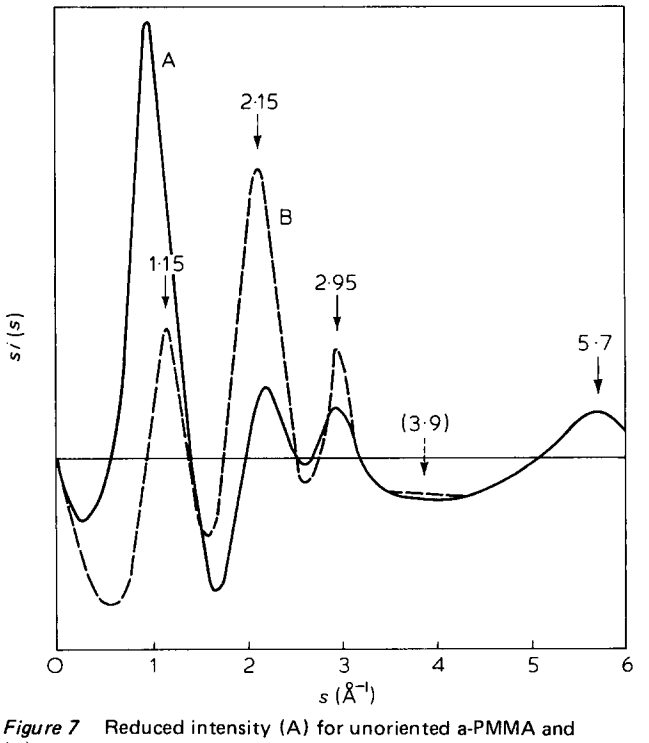

Figure 7 Reduced intensity (A) for unoriented a-PMMA and (B) meridional section for oriented a-PMMA. Intramolecular peaks are marked

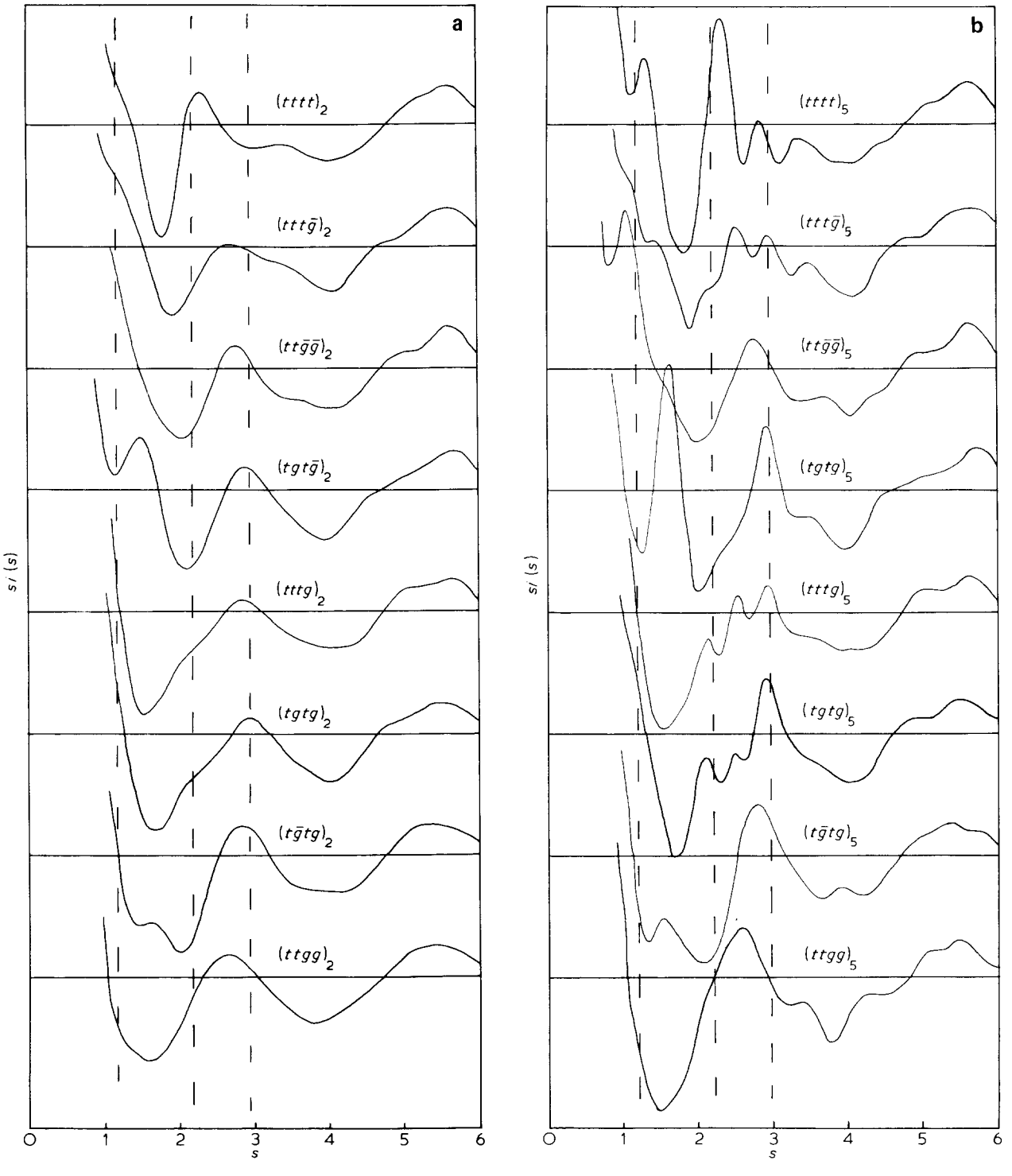

Figure 8 Calculated scattering for staggered-bond conformations from *Table 1*. Those containing more than 2 *gauche* bonds have been omitted. $\theta_1 = 110°$, $\theta_2 = 122°$. (a) 8 backbone bonds, (b) 20 backbone bonds. The vertical dashed lines indicate the position of the experimental intramolecular maxima

There is little difference between the scattering from (10°, 10°, −10°, −10°) and that from (0°, 20°, 0°, −20°), which reflects the fact that the two conformations are very similar, particularly the disposition of the sidegroups. We opt for (10°, 10°, −10°, −10°) since it has a slightly larger radius of curvature and also gives slightly lower steric hindrance between sidegroups.

Length of underlying conformation

Figure 12 shows the scattering from increasing lengths of the regular type I/II conformation (10°, 10°, −10°, −10°) with $\theta_1 = 110°$ and $\theta_2 = 128°$ which gives curved chains of radius 10–12 Å.

The splitting to give peaks at 2.2 and 3.0 $Å^{-1}$ occurs for 3 or more monomer units (6 backbone bonds) in the regular conformation, whereas the peak at ~1.2 $Å^{-1}$ only appears for lengths greater than 12 backbone bonds. Regular chains longer than about 20 backbone bonds give splitting of the 1.2 $Å^{-1}$ peak and also give too narrow peaks elsewhere. Thus it seems that regular sequences with an average length of 16–20 backbone bonds would give the best agreement with the observed scattering.

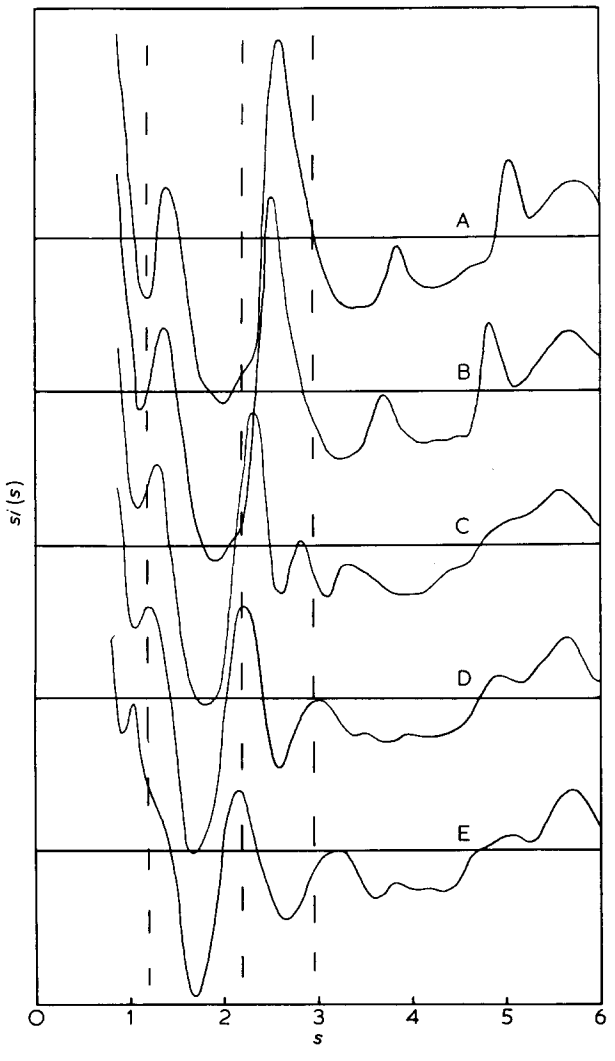

Figure 9 Effect of changes in backbone bond angles on calculated scattering for $(tttt)_5$

A, $\theta_1 = \theta_2 = 110°$
B, $\theta_1 = \theta_2 = 116°$
C, $\theta_1 = 110°, \theta_2 = 122°$
D, $\theta_1 = 110°, \theta_2 = 128°$
E, $\theta_1 = 100°, \theta_2 = 125°$

Ester rotation angles

As we have discussed earlier[22], the evidence from spectroscopy[8] and from energy calculations is that the ester group is approximately coplanar with the CH_3–C^{α}–C^{ester} bonds, so that $\omega \sim 0°$ and $\chi \sim 0°$ or 180°. There is disagreement as to which value of χ is favoured.

Since the only appreciable change of atom positions between $\chi = 0°$ and $\chi = 180°$ is the movement of the ester methyl group (one-sixth of the total number of electrons), the difference in scattering is mainly in peak heights rather than peak positions (*Figure 13*). However $\chi = 180°$ does give a marked peak at $s = 4.0$ Å^{-1} which is not observed. Hence it seems that $\chi = 0°$ predominates.

The maximum deviation from the 'coplanar' positions is likely to be $\sim 30°$. The curve for χ taking random values of $+30°$ or $-30°$ in *Figure 13* shows that such a deviation would displace the peaks whilst leaving the general shape of the pattern similar.

DISCUSSION

Summary of proposed conformation

The underlying conformation proposed is in substantial agreement with predictions from other less direct experimental techniques and from conformational energy calculations, particularly those of Sundararajan and Flory[19]. The backbone is near to the all-*trans* conformation which has been inferred from infra-red measurements[8,9]. More precisely it is near (10°, 10°, −10°, −10°) in which the dyads have the same conformation as the lowest minimum found by Sundararajan and Flory, and is one of the minima (although not the lowest) found by Grigoreva *et al.*[17].

The splitting of the intramolecular scattering into peaks at $s = 2.2$ and 3.0 Å^{-1} is seen to be a direct consequence of the curvature of the molecule due mainly to the unequal backbone bond angles. The analysis suggests that these angles should differ by a larger amount than previously proposed[19] (i.e. 110°, 128° rather than 110°, 122°). These unequal angles lead to a curved chain with a radius of 10–12 Å. The analysis also indicates that regular conformational sequences persist for 16–20 backbone bonds, supporting predictions made on the basis of measurements of characteristic ratio and interpretation of the form of small-angle scattering using X-rays for solutions and neutrons for tagged solids[7].

Of the two likely rotational positions for the ester sidegroups, the WAXS evidence is that the energy mi-

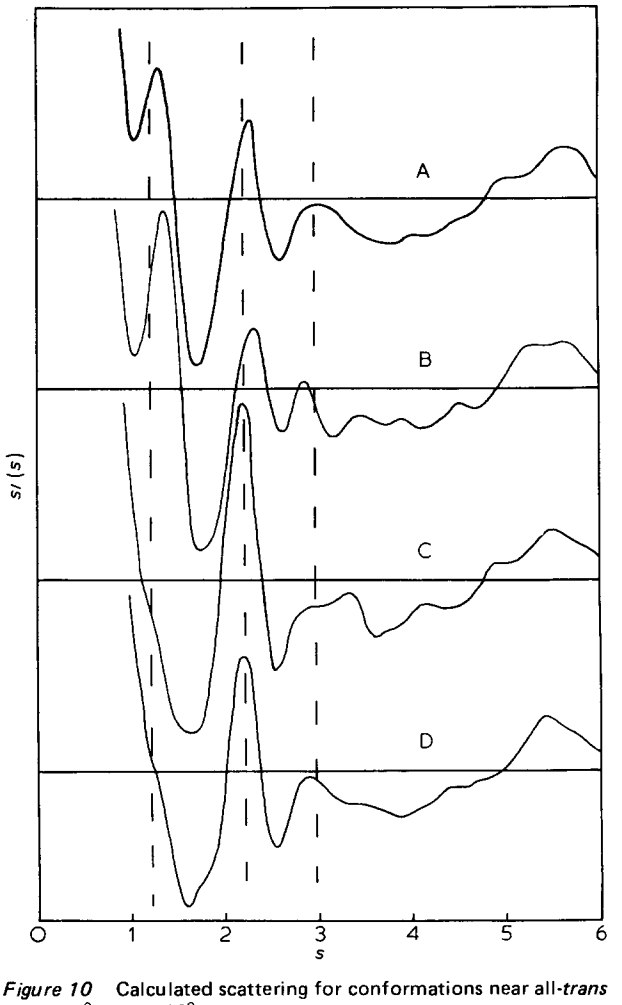

Figure 10 Calculated scattering for conformations near all-*trans* $\theta_1 = 110°, \theta_2 = 128°$

(A) $(0°, 20°, 0°, -20°)_5$ Type I
(B) $(20°, 20°, -20°, -20°)_5$ Type I/II
(C) $(-20°, -20°, 20°, 20°)_5$ Type I/II
(D) $(20°, 20°, 20°, 20°)_5$ Type II

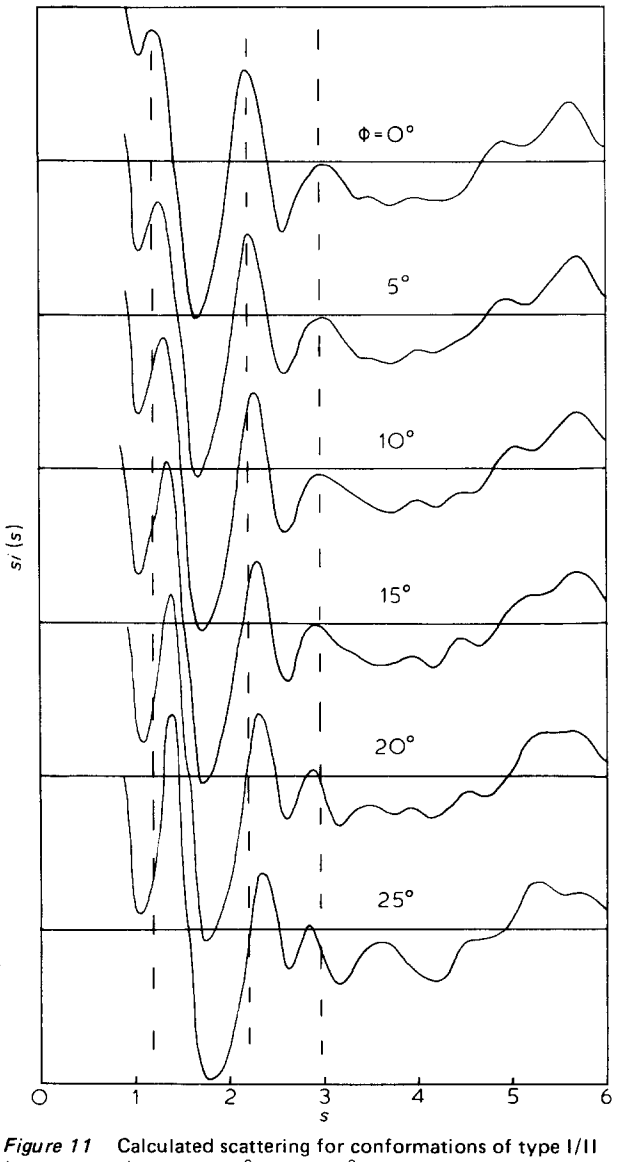

Figure 11 Calculated scattering for conformations of type I/II $(\phi, \phi, -\phi, -\phi)_5$. $\theta_1 = 110°, \theta_2 = 128°$

nimum near to $\chi = 0°$ is the most populated. This agrees with Sundararajan and Flory[19] and with Grigoreva and Goglib[17], but is opposite to the findings of Japanese workers[18,23,24] who report that $\chi = 180°$ is preferred.

We have stated the conformational conclusions in terms of precise values for the bond angles and rotation angles, whereas in a polymer at room temperature there will be thermal oscillations about the minimum energy positions. To see what effect such oscillations would have on the scattering, we calculated $si(s)$ for the preferred conformation but with random variations of $\pm 2°$ for the bond angles and $\pm 5°$ for the rotation angles. The difference from $si(s)$ for the fixed conformation is barely perceptible and if curves are plotted on the same axes they are indistinguishable. Thus the conformational angles quoted are taken as representing the average values for the vibrating molecule. Furthermore, it should be realized that although the conformational parameters quoted are those which are most probable, transitions to less probable states can occur at frequencies dependent on the energy barrier involved.

Scattering from oriented chains

A further check on the proposed model is provided by comparing WAXS data from oriented a-PMMA with the cylindrically-averaged scattering calculated for the model. The WAXS pattern for PMMA that has been deformed to an extension ratio of ~3:1 at 100°C is shown as $si(s, \psi)$ in *Figure 3*. Randomization of such patterns[25] has shown that conformational changes during orientation are small and hence we can use data from oriented specimens to give further information on the conformation in the unoriented state.

The scattering, $si(s, \psi)$, for the model is cylindrically averaged about the segment axis (for curved chains this is taken to be the tangent to the midpoint of the segment) by calculating[26]:

$$i(R, Z) = \sum_n \left[\sum_j f_j(s) J_n(Rr_j) \cos(Zz_j - n\varphi_j) \right]^2 + \sum_n \left[\sum_j f_j(s) J_n(Rr_j) \sin(Zz_j - n\varphi_j) \right]^2 - \sum_j f_j^2(s)$$

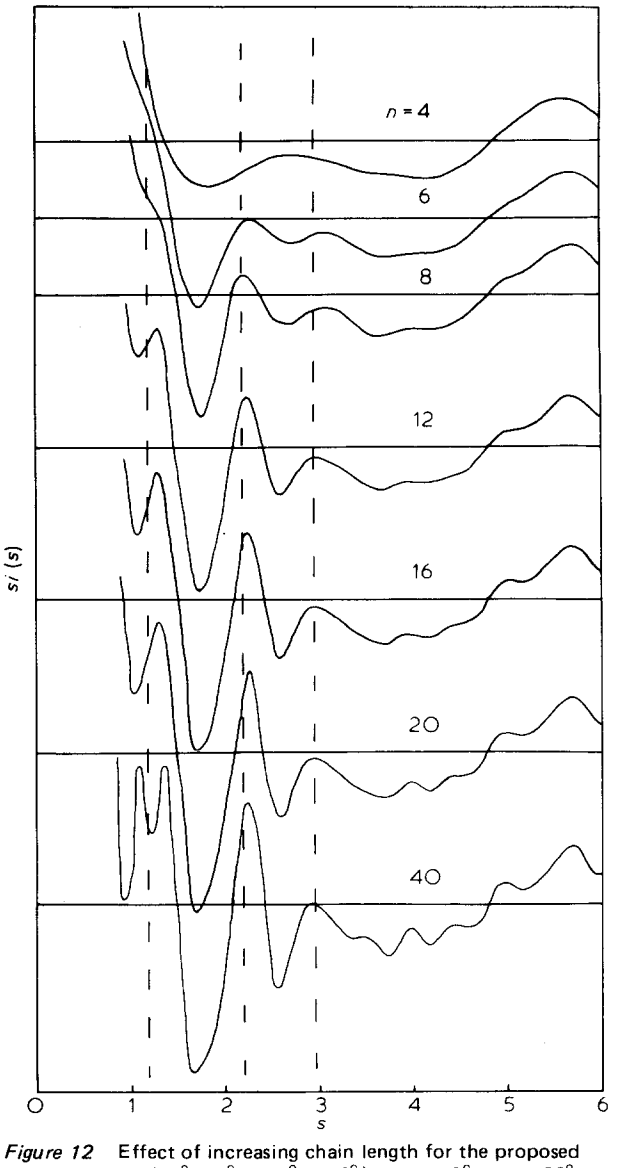

Figure 12 Effect of increasing chain length for the proposed conformation. $(10°, 10°, -10°, -10°)$ $\theta_1 = 110°, \theta_2 = 128°$, n = number of backbone bonds

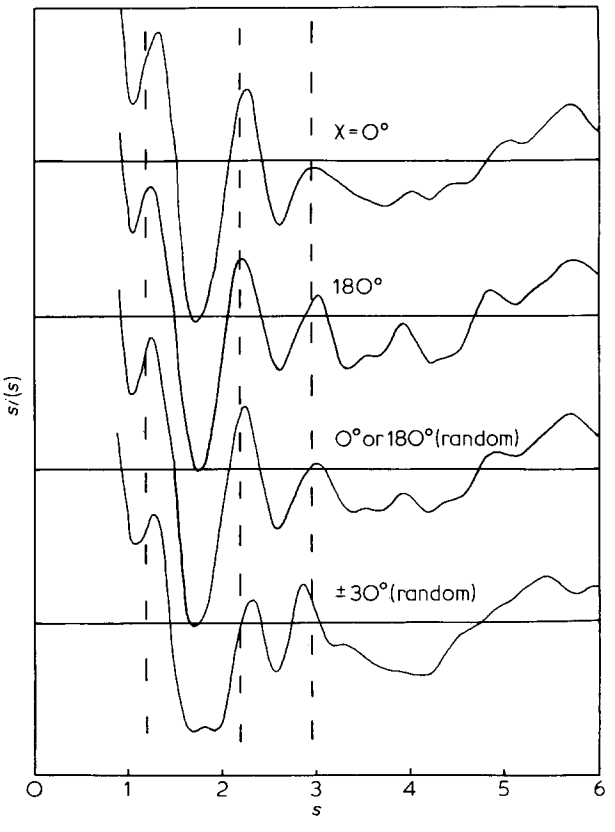

Figure 13 Effect of ester rotation for the proposed conformation: $(10°, 10°, -10°, -10°)_5$. $\theta_1 = 110°, \theta_2 = 128°$

where $R = s\cos\psi$, $Z = s\sin\psi$, J_n is the Bessel function of order n (we used $n = -5$ to $+5$), and (r_j, z_j, φ_j) are the cylindrical coordinates of the jth atom with respect to the segment axis. All hydrogen atoms have been ignored in these calculations.

Again, there would be a large peak near the origin caused by the finite size of the model but this time we corrected for it. This was done by subtracting

$$si(R, 0) \times \left(\frac{\sin cZ}{cZ}\right)^2$$

which is the scattering from a prism with length $(2c)$ equal to that of the model and with the same radial structure, but with no structure in the z-direction.

Figure 14 shows the scattering calculated for the proposed model. The peak positions of the non-equatorial haloes of the experimental pattern (*Figure 3*) are drawn in as dashed lines. The calculated pattern has more detail than the experimental since the calculations are effectively for perfectly aligned molecular segments. However, the two patterns are in broad agreement, with meridional arcs at 2.2 and 3.0 $Å^{-1}$, and with a diffuse off-meridional peak near 1.2 $Å^{-1}$ which is apparent only in the azimuthally sharpened version of the experimental pattern (*Figure 5*).

Relationship between scattering pattern and molecular structure

The main features of the scattering pattern can be accounted for by examination of the proposed model, schematic diagrams of which are shown in *Figure 15*. Each of the three main diffraction maxima can be related to important periodicities in the molecule. *Figure 15a* represents a segment of syndiotactic molecule in the proposed conformation, looking at the outside surface of the curved chain. The length of the segment, 16 backbone bonds, corresponds to the predicted average length of regular conformation. The first intramolecular peak at $s = 1.2$ $Å^{-1}$ is the one which is clearly off-meridional with an azimuthal angle in the region of 45°. The periodicity (5.2 Å) corresponding to this peak is superimposed on the molecular sketch in *Figure 15a* to give a fair indication of its origins. It is noteworthy that if the bent planar conformation were to be distorted into a slowly turning helix then such correspondence would be lost. This would account for the near-absence of the first maximum in the calculated scattering for the helix of the form (20°, 20°, 20°, 20°) in *Figure 10*.

Figure 15b, a repeat of the molecular sketch of *Figure 15a*, shows that the periodicity of 2.85 Å derived from the second intramolecular peak, which concentrates on the meridian for oriented specimens, corresponds to the average repeat between ester groups as projected onto the segment axis (i.e. tangent to the midpoint of the molecular segment). It can be seen that the repeat is longer than the 2.5 Å axial repeat distance typical of a molecule in a near all-*trans* conformation, and that this is a direct result of the curvature of the chain. *Figure 15c*, which is a sketch of the proposed conformation viewed normal to the plane of curvature, demonstrates this effect. It also shows that a repeat of 2.15 Å indicated by the third halo can be accounted for by the carbon–second carbon distance along the backbone, again projected onto the segment axis. It is apparent that the foreshortening which occurs in the projection of a curved molecule onto the axis is primarily responsible for the average carbon–second carbon axial repeat being less than 2.5 Å. The diagram (*Figure 15c*) also illustrates why the calculated scattering showed the position of the second halo to be particularly sensitive to the difference between alternate bond angles (*Figure 9*).

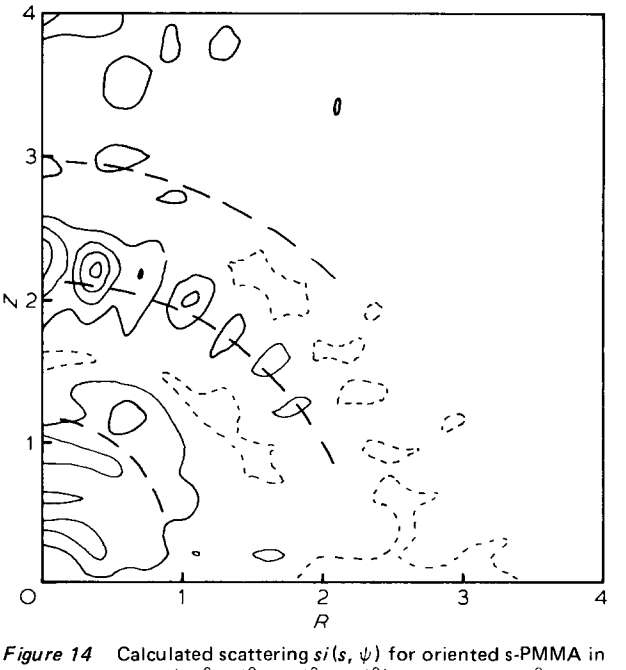

Figure 14 Calculated scattering $si(s, \psi)$ for oriented s-PMMA in the conformation $(10°, 10°, -10°, -10°)_5$ with $\theta_1 = 110°$ and $\theta_2 = 128°$. – – – – – – Negative contours, —— —— —— Non-equatorial haloes from experimental pattern

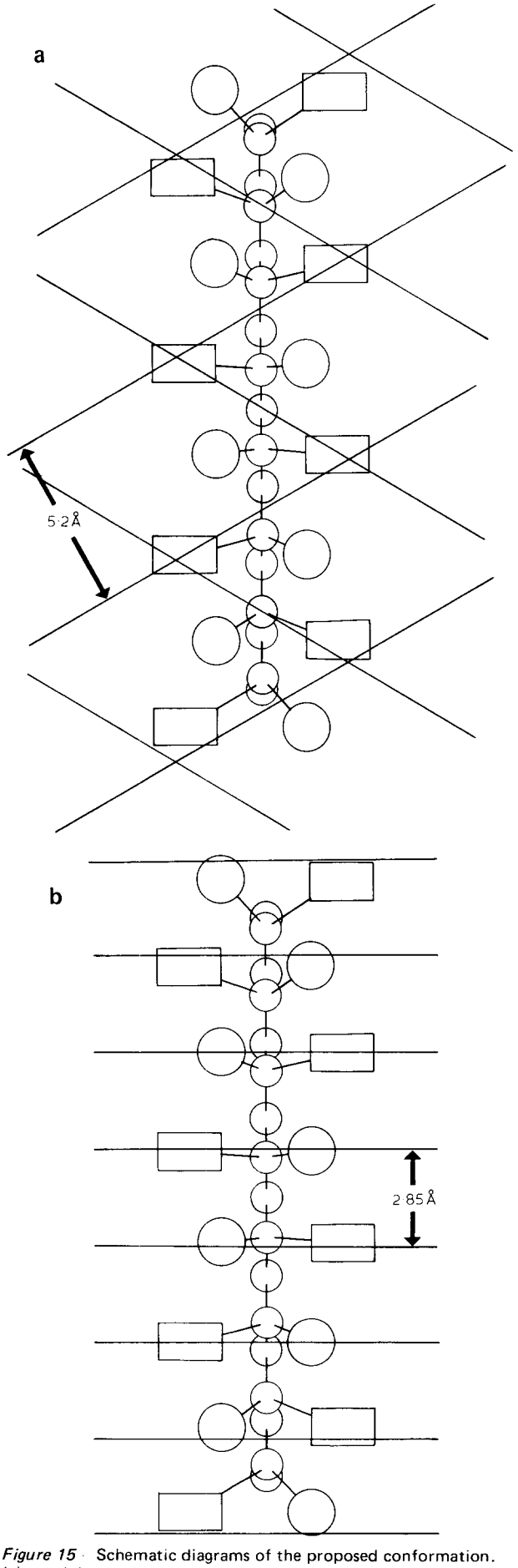

Figure 15 Schematic diagrams of the proposed conformation. (a) and (b) looking at outside surface of curved chain, (c) viewed normal to plane of curvature. Smaller circles represent backbone carbon atoms, larger circles the methyl groups, and boxes the ester groups

Stereoregularity

In this work we have related the scattering from atactic PMMA to models of syndiotactic molecules. The justification for this comparison is based on the facts: that the atactic material used contains around 80% syndiotactic dyads, that the X-ray scattering from this atactic PMMA and from syndiotactic material are virtually indistinguishable (*Figure 1*) and that the scattering from even highly isotactic PMMA is not particularly different. In broad terms therefore it appears that the conformation of PMMA remains close to all-*trans* whatever the tacticity. Computer programs to build and transform non-stereoregular chains are currently in use to explore in detail the effect of tacticity. This further work will be reported in due course.

Crystalline syndiotactic PMMA

In any study of the conformation of a non-crystalline polymer which is either stereoregular or nearly so, knowledge of the corresponding crystal structure can provide useful guidance. For s-PMMA however we know of no reports of the achievement of thermal crystallization and our own experiments were equally unsuccessful. Work which has demonstrated that solution crystallization is possible[27,28] may not be particularly relevant as there is some indication that solvent must necessarily be present, since attempts to remove it completely have led to a loss of the crystallinity. We suggest that the reason for the reluctance of s-PMMA to crystallize is associated with the curvature of the molecule proposed here. Thus for s-PMMA, despite the stereoregularity of the molecule, it appears that the amorphous state is more stable than the crystalline at all temperatures.

CONCLUSIONS

(1) Of the three prominent broad peaks in the wide-angle X-ray scattering from atactic PMMA, the first is composite containing an intermolecular component at $s = 0.95$ Å^{-1} and an intramolecular component at 1.2 Å^{-1}, whereas both the second at 2.2 Å^{-1} and the third at 2.95 Å^{-1} are intramolecular in character.

(2) Two-dimensional scattering patterns from oriented specimens show that the intramolecular component of the first peak is at an azimuthal angle of approximately 45°. The second and third intramolecular peaks concentrate on the meridian.

(3) The X-ray scattering from commercial a-PMMA containing around 80% racemic dyads is very similar to that from s-PMMA.

(4) Calculations of the scattering from a range of sterically viable conformations shows that only structures near to the all-*trans* energy minimum are compatible with the experimental data.

(5) Optimization of backbone rotation angles near to all-*trans*, backbone bond angles and ester-group rotation angles so as to give the best fit to the WAXS data leads us to propose the following underlying conformation:

Backbone rotation angles	(10°, 10°, −10°, −10°)
Backbone bond angles	$\theta_1 = 110°$, $\theta_2 = 128°$
Ester group rotation	$\chi = 0°$ dominant
Mean run length for underlying conformation (for s-PMMA)	16–20 backbone bonds

(6) This model, proposed on the basis of wide-angle X-ray analysis, is in accord with the predictions of the conformational energy calculations of Sundararajan and Flory[19], and the mean run length of the underlying conformation falls within the range indicated by small-angle X-ray and neutron scattering[7].

(7) The marked difference between alternate backbone bond angles leads to a curved molecule, and it is possible that this is the reason why syndiotactic PMMA cannot be thermally crystallized.

ACKNOWLEDGEMENTS

The authors wish to thank Geoffrey Mitchell and Richard Waring for their association with the work, Professor R. W. K. Honeycombe for the provision of facilities and the Science Research Council for funding (GR/A 13387). In addition we are most grateful to Dr. K. Nakatsuka of Mitsubishi Rayon Company, Dr. K. Hatada of Osaka University, Drs. F. Bosscher and E. Roerdink of the State University of Groningen and Dr. E. Gipstein of IBM, San Jose for the gifts of stereoregular samples.

REFERENCES

1 Bjornhaug, A., Ellefsen, O. and Tonnesen, B. A. *J. Polym. Sci.* 1954, **12**, 621
2 Wecker, S. M., Davidson, T. and Cohen, J. B. *J. Mater. Sci.* 1972, **7**, 1249
3 Voigt-Martin, I. and Mijlhoff, F. C. *J. Appl. Phys.* 1976, **47**, 3942
4 Arndt, U. W. and Riley, D. P. *Phil. Trans. Roy. Soc.* 1955, **247A**, 409
5 Lovell, R., Mitchell, G. R. and Windle, A. H. *Faraday Discussion* 1980, **68**, 46
6 Kirste, R. G., Kruse, W. A. and Ibel, K. *Polymer* 1975, **16**, 120
7 Yoon, D. Y. and Flory, P. J. *Macromolecules* 1976, **9**, 299
8 Havriliak, S. and Roman, N. *Polymer* 1966, **7**, 387
9 Schneider, B., Stokr, J., Dirlikov, S. and Mihailov, M. *Macromolecules* 1971, **4**, 715
10 Inoue, Y. and Konno, T. *Makromol. Chem.* 1978, **179**, 1311
11 Waring, J. R., Lovell, R., Mitchell, G. R. and Windle, A. H. Submitted to *J. Mater. Sci.*
12 Lovell, R. and Windle, A. H. *Polymer* 1976, **17**, 488
13 Mitchell, G. R. and Lovell, R. *Acta Crystallogr. (A)* 1981, **37**, in press
14 Bovey, F. A. 'High Resolution NMR of Macromolecules' Academic Press, New York, 1972
15 Bovey, F. A. and Tiers, G. V. D. *J. Polym. Sci.* 1960, **44**, 173
16 Higgins, J. S., Allen, G. and Brier, P. N. *Polymer* 1972, **13**, 157
17 Grigoreva, F. P., Birshtein, T. M. and Gotlib, Yu. Ya. *Polym. Sci. USSR* 1967, **9**, 650; 1968, **10**, 396
18 Tanaka, A. and Ishida, Y. *J. Polym. (Polym. Phys. Edn.)* 1974, **12**, 335
19 Sundararajan, P. R. and Flory, P. J. *J. Amer. Chem. Soc.* 1974, **96**, 5025
20 Warren, B. E. 'X-ray Diffraction' Addison-Wesley, Reading, Mass., 1969, p. 117
21 Narten, A. H. *J. Chem. Phys.* 1979, **70**, 299
22 Lovell, R. and Windle, A. H. in 'Diffraction Studies on Non-Crystalline Substances' Eds. I. Hargittai and W. J. Orville-Thomas, Akademiai Kiado, Budapest
23 Tadokoro, H., Chatani, Y., Kusanagi, H. and Yokoyama, M. *Macromolecules* 1970, **3**, 441
24 Shindo, H. *J. Sci. Hiroshima Univ. Ser. A-II* 1969, **33**, 189
25 Colebrooke, A. and Windle, A. H. *J. Macromol. Sci.-Phys.* 1976, **B12**, 373
26 Davies, D. R. and Rich, A. *Acta Cryst.* 1959, **12**, 97
27 Buter, R., Tan, Y. Y. and Challa, G. *J. Polym. Sci. (Polym. Chem. Edn)* 1973, **11**, 2975
28 Vorenkamp, E. J., Bosscher, F. and Challa, G. *Polymer* 1979, **20**, 59